Ultrasonics Sonochemistry 28 (2016) 382–392

Contents lists available at ScienceDirect

Ultrasonics Sonochemistry

journal homepage: www.elsevier.com/locate/ultson

Experimental and numerical investigation of the effect of liquid temperature on the sonolytic degradation of some organic dyes in water

Slimane Merouani [a,b,*], Oualid Hamdaoui [a], Zineb Boutamine [a], Yacine Rezgui [c], Miloud Guemini [c]

[a] Laboratory of Environmental Engineering, Department of Process Engineering, Faculty of Engineering, Badji Mokhtar – Annaba University, P.O. Box 12, 23000 Annaba, Algeria
[b] Department of Chemical Engineering, Faculty of Process Engineering, University of Constantine 3, Constantine, Algeria
[c] Laboratory of Applied Chemistry and Materials Technology, University of Oum El-Bouaghi, P.O. Box 358, 04000 Oum El Bouaghi, Algeria

ARTICLE INFO

Article history:
Received 3 July 2015
Received in revised form 23 August 2015
Accepted 23 August 2015
Available online 24 August 2015

Keywords:
Sonochemical degradation
Organic dyes
Liquid temperature
Numerical simulations
·OH radical

ABSTRACT

This paper presents a comprehensive experimental and numerical investigation of the effects of liquid temperature on the sonochemical degradation of three organic dyes, Rhodamine B (RhB), Acid orange 7 (AO7) and Malachite green (MG), largely used in the textile industry. The experiments have been carried out for an ultrasonic frequency of 300 kHz. The obtained experimental results were discussed using a new approach combining the results of single-bubble event and the number of active bubbles. The single-bubble event was predicted using a model that combines the bubble dynamics with chemical kinetics occurring inside a bubble during the strong collapse. The number of active bubbles was predicted using a method developed in our previous work. The experiments showed that the degradation rate of the three dyes increased significantly with increasing liquid temperature in the range 25–55 °C. It was predicted that the main pathway of pollutants degradation is the attack by ·OH radicals. The simulations showed that there exists an optimum liquid temperature of about 35 °C for the production of ·OH inside a bubble whereas the number of active bubbles increased sharply with the rise of the liquid temperature. It was predicted that the overall production rate of ·OH increased with increasing liquid temperature in the range 25–55 °C. Finally, it was concluded that the effect of liquid temperature on the sonochemical degradation of the three dyes in aqueous phase was controlled by the number of active bubbles in the range 35–55 °C and by both the number of bubbles and the single bubble yield in the range 25–35 °C.

1. Introduction

Over the past two decades, sonochemical degradation of organic pollutants in water has been extensively investigated as an advanced oxidation technology [1–5]. The chemical effects of sonication (namely sonochemistry) arise from acoustic cavitation, that is, the formation, growth and implosive collapse of tiny bubbles in a liquid irradiated by ultrasonic waves [6]. Fast collapse of the bubbles adiabatically compresses entrapped vapor and gas, which results in short and local hot spots with enormous conditions [7]. At the final step of the collapse, the temperature and pressure inside the bubble attained several thousand of Kelvin and several hundreds of atmosphere, respectively [8,9]. These extremely high conditions formed in collapsing bubbles lead to the thermal dissociation of the trapped water vapor into reactive hydroxyl radicals (·OH) and hydrogen atoms (H·) [10]. These active species can recombine, react with other gaseous species present in the cavity, i.e. O_2, to form other active species such as HO_2 and O, or diffuse out of the bubble into the bulk liquid medium where they are able to induce chemical transformation [11]. Three zones of distinct reactivity appear during the collapse event [12]: the interior of the bubble, the gas–liquid interface and the bulk liquid solution. As a result, an organic pollutant with high volatility character (high value of Henry's Law constant) will be incinerated in the bubble [12]. A hydrophilic or hydrophobic compound with low volatility cannot enter the bubble, but will be oxidized in the bulk solution or interfacial area by reaction with ·OH radicals ejected from the cavitation bubble [12].

In the absence of any solute in the liquid medium, the primary radicals of sonolysis mostly recombine at the bubble solution interface to form hydrogen peroxide (H_2O_2) that is released in the medium according to the following reactions [13]:

$$2{\cdot}OH \rightarrow H_2O_2 \quad k_1 = 5.5 \times 10^9\ M^{-1}\ s^{-1} \tag{1}$$

$$2{\cdot}OOH \rightarrow H_2O_2 + O_2 \quad k_2 = 8.3 \times 10^5\ M^{-1}\ s^{-1} \tag{2}$$

* Corresponding author at: Department of Chemical Engineering, Faculty of Process Engineering, University of Constantine 3, Constantine, Algeria.
E-mail addresses: s.merouani@yahoo.fr, s.merouani03@gmail.com (S. Merouani).

http://dx.doi.org/10.1016/j.ultsonch.2015.08.015
1350-4177/

Nomenclature

c	speed of sound in the liquid medium (m s^{-1})
f	frequency of ultrasonic wave (Hz)
I_a	acoustic intensity of ultrasonic irradiation (W m^{-2})
N	number of bubbles collapsing per unit volume per unit time (L^{-1} s^{-1})
$n_{H_2O_2}$	number of moles of H_2O_2 released by the collapse of single bubble (mol)
$n_{\cdot OH}$	number of moles of ·OH released by the collapse of single bubble (mol)
$n_{HO_2^\cdot}$	number of moles of HO_2 released by the collapse of single bubble (mol)
p	pressure inside a bubble (Pa)
p_∞	ambient static pressure (Pa)
P_A	amplitude of the acoustic pressure (Pa)
P_v	vapor pressure of water (Pa)
P_{g0}	initial gas pressure (Pa)
R	radius of the bubble (m)
R_{max}	maximum radius of the bubble (m)
R_{min}	minimum radius of the bubble at the collapse (m)
R_0	ambient bubble radius (m)
t	time (s)
T	temperature inside a bubble (K)
T_∞	ambient liquid temperature (K)

Greek letters

γ	specific heat ratio (c_p/c_v) of the gas mixture
σ	surface tension of liquid water (N m^{-1})
ρ	density of liquid water (kg m^{-3})
μ	viscosity of liquid water (N m^{-2} s)

Sonochemical reactions can be affected in several ways. Frequency, power and nature of the dissolved gas have been largely studied in the past and their important effects on the reaction rate have been shown [13–17]. Moreover, previous studies [18–21] have demonstrated that the temperature of the sonicated solution have a significant impact on the reaction rate. However, to the best of our knowledge, there is no study explaining quantitatively the effect of liquid temperature on the sonochemical reaction rate.

Dye removal from industrial effluents has been the subject of great attention in the last few years. Approximately, 10–15% of the overall production of dyes is released into the environment, mainly via wastewater [20]. The presence of low concentration of dyes in the effluent streams is highly visible and it reduces the light penetration that leads to inhibiting photosynthesis and stringent restrictions on the organic content of industrial effluents [20].

In this work, the dyes under consideration are Rhodamine B (RhB), Acid orange 7 (AO7) and Malachite green (MG). RhB is a basic dye of the xanthene class. It is widely used in industrial purposes as a colorant in textile, leather, jute and food industries, and is also a well-known water tracer fluorescent [21]. It is harmful if swallowed by human beings and animals, and causes irritation to the skin, eyes, gastrointestinal tract and respiratory tract [21]. The carcinogenicity, reproductive and developmental toxicity, neurotoxicity and chronic toxicity towards humans and animals have been experimentally proven [22]. AO7 is a mono-azo acidic dye, which is widely used in dyeing, weaving, tanning and paper industries [23] and therefore, it has wide environmental effects. MG is a basic dye of the triarylmethane class. It is most widely used for coloring purpose, amongst all other dyes of its category [24]. This dye is widely used in the aquaculture industry worldwide as a biocide as well as in the silk, wool, cotton, leather, paper, and acrylic industries as a dye. It is also employed as therapeutic agent to treat parasites, fungal and bacterial infections in fish and fish eggs and as antiseptic, but only for external applications on the wounds and ulcers [25]. Despite its extensive use, MG is a highly controversial compound due to its reported toxic properties which are known to cause carcinogenesis, mutagenesis, teratogenesis, and respiratory toxicity [26].

The main objective of this study was to clarify experimentally and numerically the effects of liquid temperature on the sonochemical degradation of RhB, AO7 and MG. A new approach combining the results of single-bubble event and the number of active bubbles was used to analyze the experimental results. The chemical single-bubble yield has been predicted using a model that combines the bubble dynamics with chemical kinetics consisting of series of chemical reactions (73 reversible reactions) occurring inside a reacting bubble whereas the number of active bubbles was predicted using a method developed in our previous work [27].

2. Materials and methods

2.1. Materials

Rhodamine B (abbreviation: RhB; C.I. Basic Violet 10; C.I. number: 45170; molecular formula: $C_{28}H_{31}N_2O_3Cl$, molecular weight: 479.01 g mol^{-1}) and Acid orange 7 (abbreviation: AO7; C.I. Orange II; molecular formula: $C_{16}H_{11}N_2NaO_4S$, molecular weight: 350.32 g mol^{-1}) were supplied by Sigma–Aldrich. The cationic dye (C.I. 42000; Basic Green 4), Malachite green oxalate salt, (abbreviation: MG; molecular formula $C_{52}H_{56}N_4O_{12}$, molecular weight: 929 g mol^{-1}), was obtained from Merck. The three dyes were used without further purification. The molecular structures of RhB, AO7 and MG are shown in Fig. 1.

Potassium iodide (KI) and ammonium heptamolybdate ($(NH_4)_6Mo_7{\cdot}4H_2O$) were procured, respectively, from Riedel-de Haën and Sigma–Aldrich.

2.2. Ultrasonic reactor

Sonolysis experiments were conducted in a cylindrical water-jacketed glass reactor (Fig. 2). The ultrasonic waves at 300 kHz were emitted from the bottom of the reactor through a piezoelectric disc (diameter 4 cm) fixed on Pyrex plate (diameter 5 cm). The temperature of the solution was monitored using a thermocouple immersed in the reacting medium. Acoustic power dissipated in the reactor was estimated using a standard calorimetric method [28,29].

2.3. Procedures

Sonochemical experiments involving dyes degradation and H_2O_2 production in pure water were carried out under different conditions using constant solution volume of 300 mL. The temperature of the aerated solution was maintained at a desired value by circulating cooling water through a jacket surrounding the cell. In all experiments, the acoustic power delivered to the reactor was fixed at 25.5 W, which yield an acoustic intensity of 2 W cm^{-2}. Aqueous samples were taken periodically from the sonicated solution and the concentration of each dye was determined using

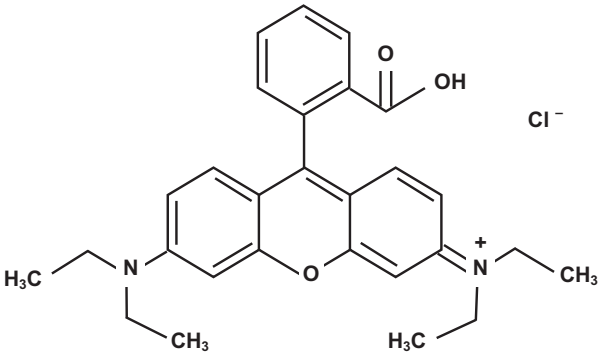

Rhodamine B (RhB)

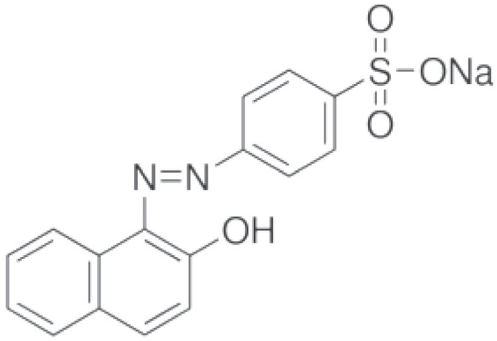

Acid orange 7 (AO7)

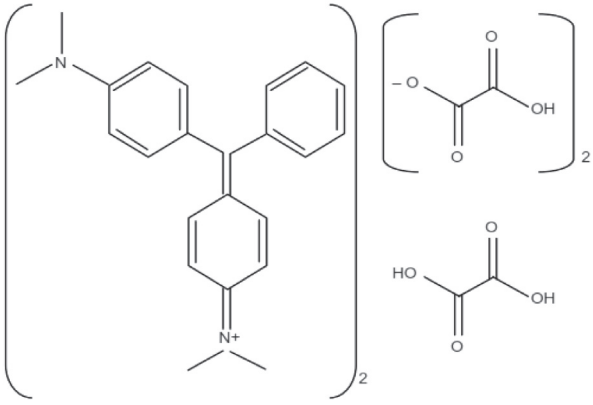

Malachite Green (MG)

Fig. 1. Molecular structures of Rhodamine (RhB), Acid orange 7 (AO7) and Malachite green (MG).

a UV–visible spectrophotometer (Jenway 6405) at the maximum wavelength (551 for RhB, 485 nm for AO7 and 618 nm for MG).

Hydrogen peroxide concentrations were analytically determined using the iodometric method [30]. Sample aliquots taken periodically from the reactor during sonolysis were added in the quartz cell of the spectrophotometer containing 1 mL of potassium iodide (0.1 M) and 20 μL of ammonium heptamolybdate (0.01 M). The iodide ion (I^-) reacts with H_2O_2 to form the triiodide ion (I_3^-). The mixed solutions were allowed to stand for 5 min before absorbance was measured. The absorbance was recorded spectrophotometrically at the maximum wavelength of the formed triiodide (I_3^-) (352 nm; the molar absorptivity ε = 26,300 L mol^{-1} cm^{-1}).

3. Theoretical package

The theoretical procedure used for analyzing the experimental results combines a model for a single bubble sonochemistry with a model for the estimation of the number of cavitation bubble in acoustic cavitation field. The following is a description of the procedure.

3.1. Single bubble sonochemistry model

The model used for studying the single bubble sonochemistry at different conditions of liquid temperature has been fully described in our previous papers [27,31,32]. The model combines the dynamic of single bubble with chemical kinetics occurring inside a bubble during the collapse. The following is a brief description of the model.

A gas and vapor filled spherical bubble isolated in water oscillates under the action of a sinusoidal sound wave. The temperature and pressure in the bubble are assumed spatially uniform and the gas content of the bubble behaves as an ideal gas [33]. The radial dynamics of the bubble is described by the Keller-Miksis equation that includes first order terms in the Mach number $M = \dot{R}/c$ [34,35]:

$$\left(1-\frac{\dot{R}}{c}\right)R\ddot{R}+\frac{3}{2}\left(1-\frac{\dot{R}}{3c}\right)\dot{R}^2=\frac{1}{\rho_L}\left(1+\frac{\dot{R}}{c}\right)\times\left[p-p_\infty-\frac{2\sigma}{R}-4\mu\frac{\dot{R}}{R}+P_A\sin(2\pi ft)\right]+\frac{R}{\rho_L c}\frac{d}{dt}\left[p-p_\infty-\frac{2\sigma}{R}-4\mu\frac{\dot{R}}{R}+P_A\sin(2\pi ft)\right] \quad (3)$$

in this equation dots denote time derivatives (d/dt), R is the radius of the bubble, c is the speed of sound in the liquid, ρ_L is the density of the liquid, σ is the surface tension, μ is the liquid viscosity, p is the pressure inside the bubble, p_∞ is the ambient static pressure, P_A is the acoustic amplitude and f is the sound frequency. The

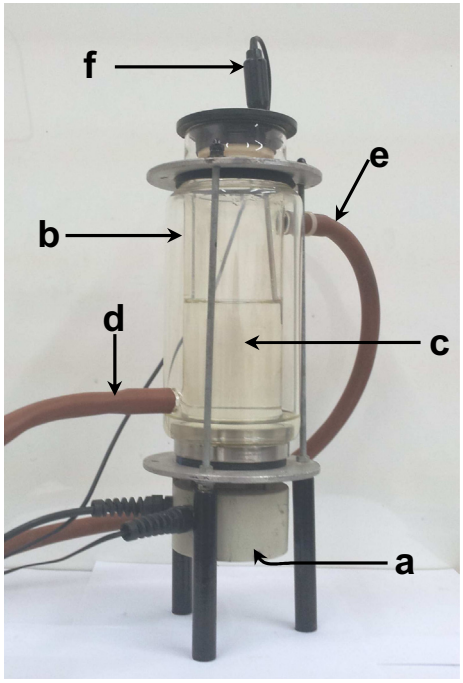

Fig. 2. Sonochemical reactor used for the sonolytic experiments. (a) 300 kHz ultrasonic transducer, (b) cylindrical jacketed glass cell, (c) sonicated solution, (d) inlet cooling water, (e) outlet cooling water, (f) thermocouple.

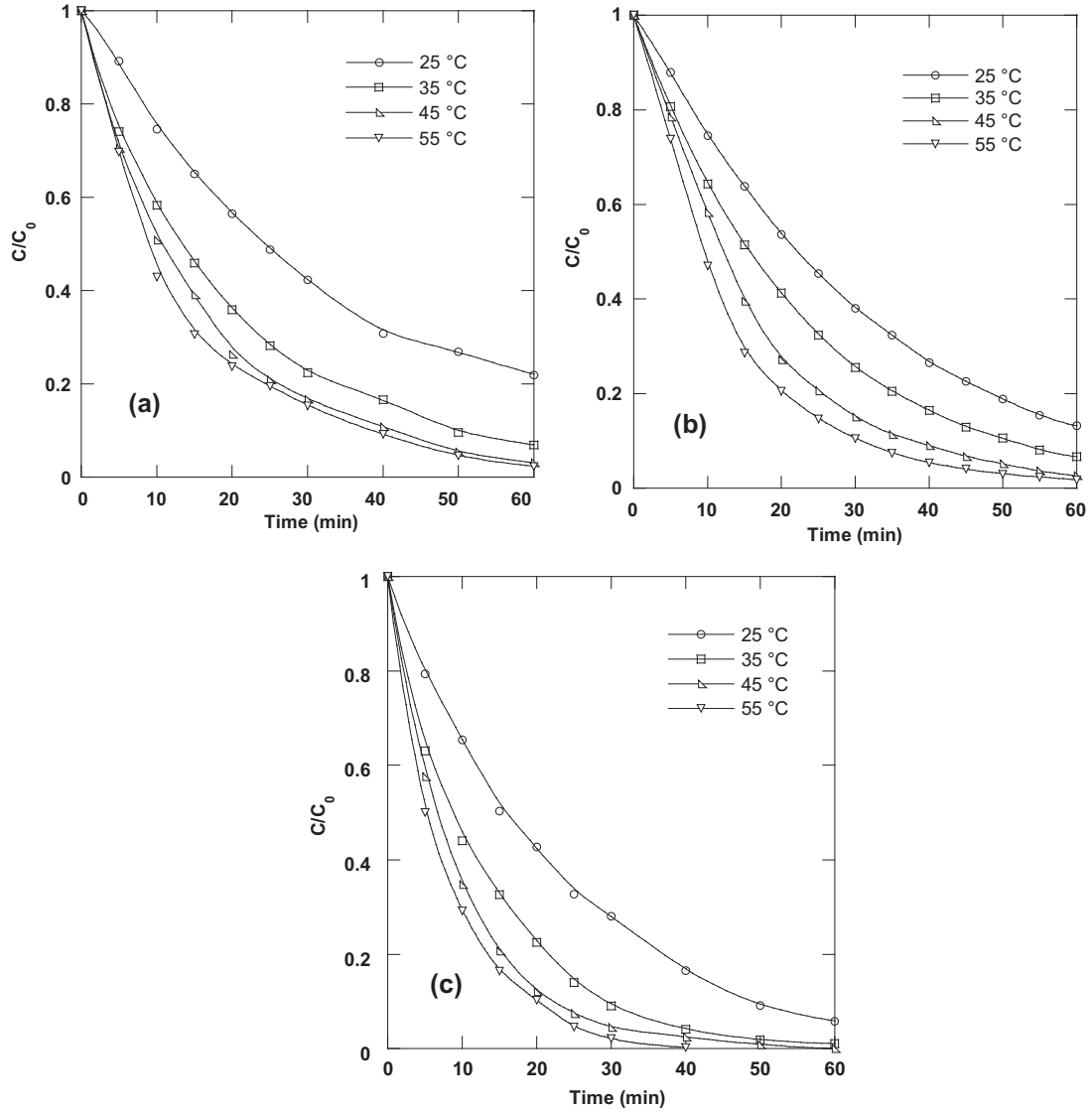

Fig. 3. Kinetics of the sonolytic removal of (a) AO7, (b) RhB and (c) MG as function of time for various liquid temperatures (conditions: initial dye concentration: 5 mg L^{-1}, volume: 300 mL, liquid temperature: 25–55 °C, frequency: 300 kHz, acoustic intensity: 2 W cm^{-2}).

acoustic amplitude P_A is correlated with the acoustic intensity I_a, or power per unit area, as $P_A = (2I_a\rho_L c)^{1/2}$ [10].

The expansion of the bubble is assumed as isothermal and its total compression is considered as adiabatic [36,37]. These assumptions, which are widely accepted since the lifetime of an oscillation at high frequency is relatively short with a very rapidly occurring collapse event, were pointed out by Yasui et al. [38] using a more detailed model. We also assume that the vapor pressure in the bubble remains constant during the bubble expansion phase and there is no gas diffusion during expansion and no mass and heat transfer of any kind during collapse. Storey and Szeri [39] demonstrated that the inclusion of mass transfer on the bubble dynamics has practically no effect on the maximum bubble temperature attained in the bubble at the collapse when the compression ratio of the bubble (R_{max}/R_{min}) is less than 20 (R_{max} is the maximum radius of the bubble and R_{min} is the minimum bubble radius at the collapse). This level of R_{max}/R_{min} was never attained in the present numerical study. Therefore, in order to reduce computational parameters, the current model takes, as input, initial bubble vapor content and neglects mass and heat transfer during bubble expansion and collapse.

Because of the above assumptions, the pressure and temperature inside the bubble at any instant during adiabatic phase can be calculated from the bubble size as

$$p = \left[P_v + P_{g0}\left(\frac{R_0}{R_{max}}\right)^3\right]\left(\frac{R_{max}}{R}\right)^{3\gamma} \tag{4}$$

$$T = T_\infty\left(\frac{R_{max}}{R}\right)^{3(\gamma-1)} \tag{5}$$

where P_v is the vapor pressure, $P_{g0} = p_\infty + (2\sigma/R_0) - P_v$ is the gas pressure in the bubble at its ambient state ($R = R_0$), R_0 is the ambient bubble radius, T_∞ is the bulk liquid temperature and γ is the ratio of specific heat capacities (c_p/c_v) of the gas/vapor mixture, given as

$$\gamma = \sum_{k=1}^{K} y_k\gamma_k \tag{6}$$

when y_k is the mole fraction of the species k at time corresponding to $R = R_{max}$ and γ_k is the ratio of specific heat capacities of the species k, which will be assumed constant.

It is important to notice that the assumption of spatial uniform pressure and temperature inside the bubble is valid as long as inertia effects are negligible and the velocity of the bubble wall is below the speed of sound in the vapor/gas mixture. This assumption was justified in detail in the paper published by Kamath et al. [40]. In addition, Yasui et al. [38] and Fujikawa and Akamatzu [41] pointed out in their complete models which include heat transfer that the bubble temperature and pressure are roughly uniform except at a very thin layer, called thermal boundary, near the bubble wall.

For simulating the chemical reactions occurring inside the bubble, a kinetic mechanism consisting in 73 chemical reactions and their backwards reactions (Table 2 in Ref. [42]) is taken into account including O_2, H_2O, $^{\cdot}OH$, $H^{\cdot}$, O, $HO_2^{\cdot}$, O_3, H_2, H_2O_2, N_2, N, NO, NO_2, NO_3, HNO_2, HNO_3, N_2O, HNO, NH, NH_2, NH_3, N_2H_2, N_2H_3, N_2H_4, N_2O_4 and N_2O_5 species.

The adopted chemical kinetics model consists of the reaction mechanism and determines the production of each species during the bubble collapse. Detailed information of the chemical kinetics model is available in our previous work [27].

The numerical procedure used for solving the bubble dynamic equation and simulating the reactions systems inside a bubble have been presented in detail in our previous works [27,32]. Briefly, the Keller–Miksis equation (Eq. (3)), describing the dynamic of the bubble, is a non-linear second-order differential equation which requires an approximate numerical method for solution. It has been solved by the fourth-order Runge–Kutta method using the initial conditions: $t = 0$, $R = R_0$ and $dR/dt = 0$. The simulation of the chemical reactions in the bubble (73 chemical reactions) starts at the beginning of the adiabatic phase (at time corresponding to $R = R_{max}$). The input parameters for solving the reaction system are the composition of the bubble on water vapor and air at the time corresponding to $R = R_{max}$, the temperature and pressure profiles in the bubble during adiabatic phase and the collapse time. These parameters are obtained by solving Eq. (3). As the bubble temperature increases during the adiabatic phase, the reaction system evolves and radicals start to form by thermal dissociation of H_2O and other molecules in the bubble. Thus, the composition of the bubble on all species expected to be present was determined at any temperature during the collapse period by solving the system of the ordinary differential equations using the finite difference method (see Ref. [27]). The computer simulation of the reactions system was stopped after the end of the bubble collapse.

3.2. Determination of the number of active bubbles

In sonochemical reaction field, there are two kinds of bubbles: actives (transient) and non-actives (stable) bubbles. Active bubbles are those responsible for the chemical effect and sonoluminescence. The chaotic nature of acoustic cavitation and the great disparity in bubble characteristics inside the cavitation field render very difficult the determination of the number of active bubble. The literature in this field is scarce, but, recently, some advanced methods based essentially on sonoluminescence have been used to estimate the active bubble number. These methods have covered a very limited range of operating parameters. In our previous paper [27], we have developed a simple semi-empirical method for predicting the number of active bubbles in cavitating medium. This method (adopted in this study) is based on two main assumptions:

- The cavitation is transient and the bubble breaks apart (fragments) at the first collapse after an initial expansion.
- The bubble contents mix directly with the liquid surrounding the bubble at the end of the collapse.

Basing on these assumptions, the number of collapsing bubbles per unit time per unit volume (N) is then easily determined using material balances for $^{\cdot}OH$, $HO_2^{\cdot}$ and H_2O_2 in the liquid phase. It is given by the following equation:

$$N = \frac{r_{H_2O_2}}{n_{H_2O_2} + 0.5(n_{^{\cdot}OH} + n_{HO_2^{\cdot}})} \quad (7)$$

where, the production rate of H_2O_2, $r_{H_2O_2}$, is determined experimentally and the entities $n_{H_2O_2}$, $n_{^{\cdot}OH}$ and $n_{HO_2^{\cdot}}$ (the number of moles of H_2O_2, $^{\cdot}OH$ and $HO_2^{\cdot}$) released by each bubble when it collapses are estimated using the single bubble sonochemistry model (Section 4.2.1).

4. Results and discussion

4.1. Degradation of RhB, AO7 and MG

The effect of liquid temperature on the sonochemical degradation of RhB, AO7 and MG was investigated by sonication of 5 mg L^{-1} of each dye solution at different temperatures in the range 25–55 °C using a constant solution volume of 300 mL. The obtained results are depicted in Fig. 3(a)–(c) in term of kinetics of degradation for respectively RhB, AO7 and MG and in Fig. 4 in term of initial degradation rate as function of liquid temperature. The initial degradation rates were computed as $\Delta C/\Delta t$ over the first minutes of sonication.

The application of ultrasound causes an exponential decrease of the dyes concentrations with time, indicating the effectiveness of sonolysis towards the degradation of these pollutants. From Figs. 3 and 4, it was clearly seen that an increase in liquid temperature in the range 25–55 °C results in a significant increase in the removal of the dyes. After 20 min of sonication, the removal efficiency of RhB increases from 46.3% to 58.7, 72.8 and 79.4% when the liquid temperature increases from 25 °C to 35, 45 and 55 °C, respectively. For AO7 and MG, the effect of liquid temperature is more pronounced. At 25 °C, 57.3% of MG were eliminated after 20 min of treatment and this fraction increased to 90% when the liquid temperature increased to 55 °C.

Fig. 4 showed that the sonochemical reaction rates of the three dyes follow the order: MG > AO7 > RhB. The raise in liquid

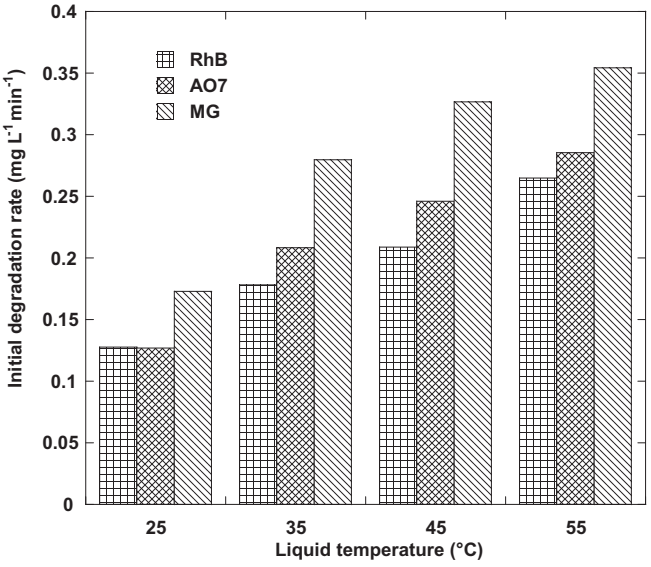

Fig. 4. Initial degradation rate of RhB, AO7 and MG as function of liquid temperature (conditions: initial dye concentration: 5 mg L^{-1}, volume: 300 mL, liquid temperature: 25–55 °C, frequency: 300 kHz, acoustic intensity: 2 W cm^{-2}).

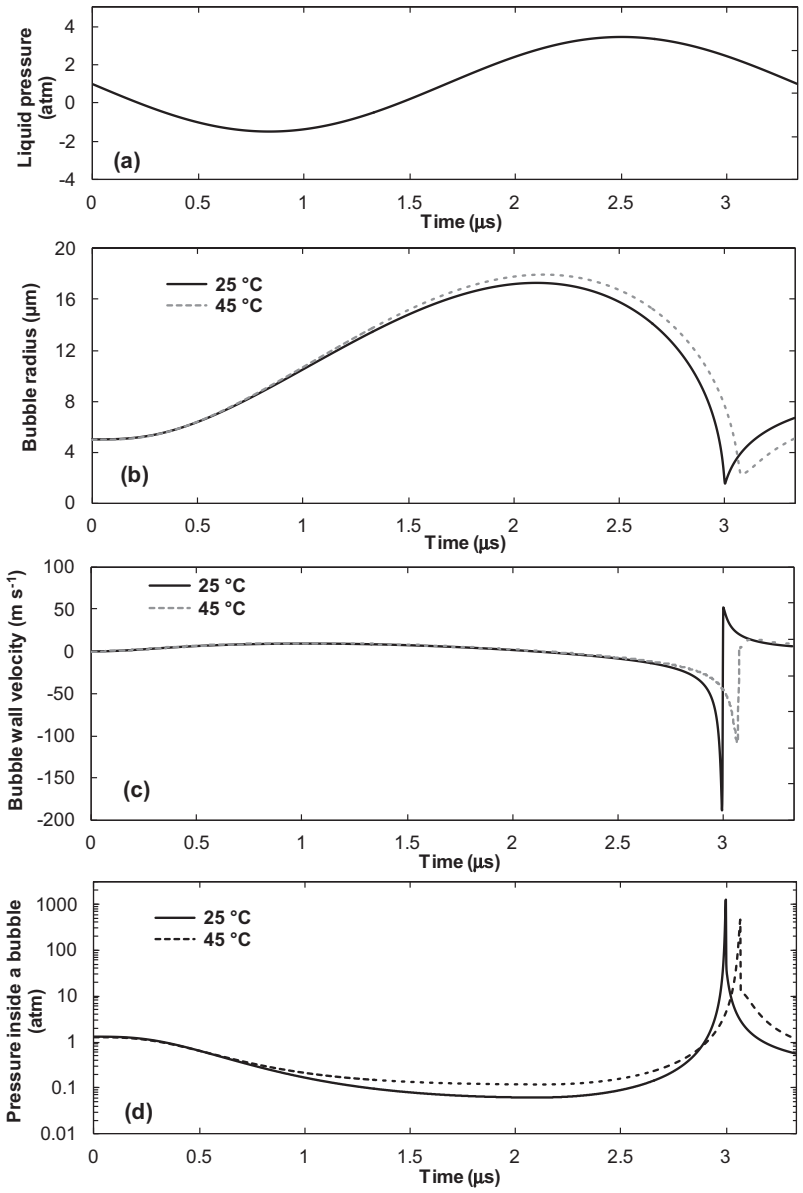

Fig. 5. The calculated liquid pressure (a) the bubble radius (b), the bubble wall velocity (c) and the pressure inside a bubble (d) as function of time for one acoustic cycle (3.33 μs) at two bulk liquid temperatures (conditions: ambient bubble radius: 5 μm, driving frequency: 300 kHz, acoustic intensity: 2 W cm^{-2}, liquid temperature: 25 and 45 °C, static pressure: 1 atm). The vertical axis in (d) is in logarithmic scale.

temperature from 25 to 55 °C results in 2-fold increase in the initial degradation rate of each dye. The rise with the liquid temperature of the degradation rate of the substrate underlined the fact that the sonochemical reactivity is higher at higher liquid temperature.

In aqueous sonochemistry, it is well established that the degradation of the pollutants is strongly depended on their physicochemical properties. An organic pollutant with high volatility character will be incinerated in the bubble whereas a hydrophilic or hydrophobic compound with low volatility will be oxidized in the bulk solution or interfacial area by reaction with ·OH radicals ejected from the cavitation bubble [13]. RhB, AO7 and MG are highly water-soluble (solubility: 120 g L^{-1} for RhB [43], 116 g L^{-1} [44] for AO7 and 40 g L^{-1} for MG [45]) and non-volatile organic compounds (Henry's law constants: 2.2×10^{-21} atm m^3 mol^{-1} for RhB [43], 7.01×10^{-17} atm m^3 mol^{-1} for AO7 [46] and 1.9×10^{-14} atm m^3 mol^{-1} for MG [47]). Therefore, these pollutants cannot enter the bubble but must be degraded at the outside of the bubble by reaction with ·OH radical ejected from the inside of the acoustic bubble. This was already confirmed in the case of RhB by the formation of hydroxylated intermediates during sonication of RhB solution [48].

MG degrades faster than AO7 and RhB because of its lower solubility and higher fugacity (higher Henry law constant), and so it accumulates at higher concentration at the bubble/solution interface where the concentration of ·OH radical is relatively high [19].

To confirm the positive effect of increasing liquid temperature toward the sono-reactivity of the dyes solutions with ·OH radicals, the concentration of H_2O_2 accumulated in a sonicated water, which is widely used as an indicator for quantifying the amount of ·OH ejected from the bubbles (reactions (1) and (2), $k_1 \gg k_2$), was monitored for various liquid temperatures under the same conditions of the degradation experiments. In all these experiments, it was found that the concentration of H_2O_2 in the sonicated medium increased linearly with sonication time (data not shown).

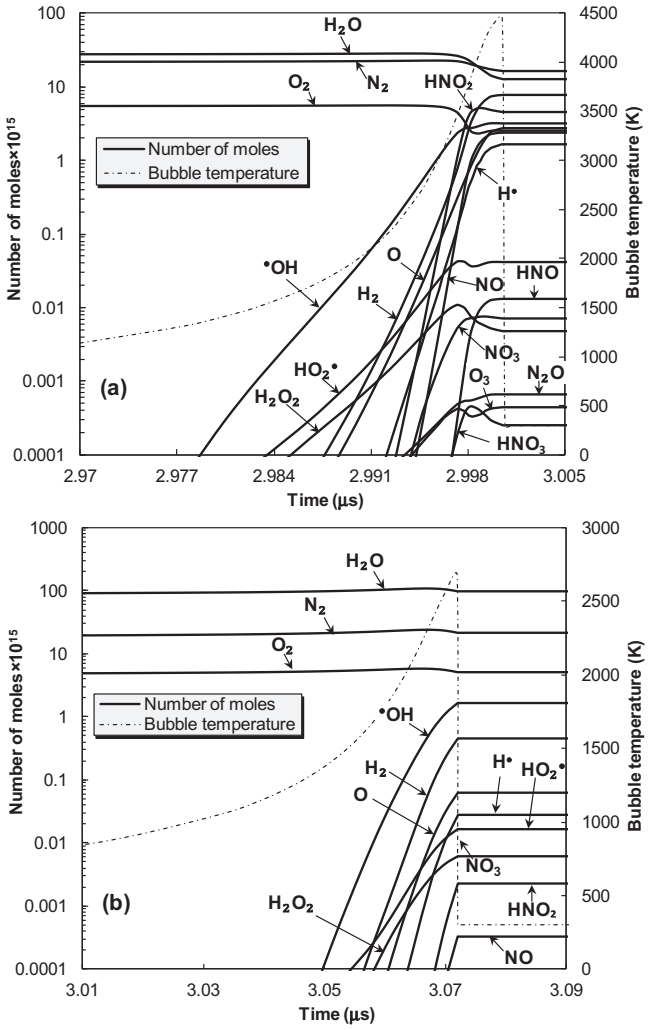

Fig. 6. Reaction system evolution inside a bubble as function of time at around the end of the bubble collapse for two different bulk liquid temperatures, (a) 25 °C and (b) 45 °C, and for the same condition as in Fig. 5. The principal vertical axes in (a) and (b) are in logarithmic scale. The horizontal axes are only for about 0.08 μs in (a) and 0.035 μs for (b). The numerical simulation of chemical reactions was conducted for a bubble initially composed of air and water vapor.

The production rate of H_2O_2 with respect to the liquid temperature is shown in Table 3. From the results of Table 3, it can be concluded that the sonochemical activity in the liquid phase increases with increasing liquid temperature in the range 25–55 °C through a rise in the production rate of hydroxyl radicals from the acoustic bubbles, resulting in higher degradation rates of the dyes.

4.2. Numerical interpretations

The efficacy of the sonochemical process depends on the cavitation process occurring in the liquid, which in turn depends on the combined effect of individual cavities and their number. Any effort to estimate the chemical content of a collapsing single-bubble and the number of active bubbles under various liquid temperatures could yield important information, at least qualitatively, about the factors that govern the overall degradation rate of the dyes with respect to the liquid temperature. Therefore, the objective of this section is to interpret the experimental results of Fig. 4 by estimating the chemical content of a collapsing single-bubble, i.e. amount of ·OH radical, and the number of active bubbles under the same experimental conditions. The model described in Section 3.1 has been used to study the single bubble sonochemistry whereas the number of active bubbles was predicted according the method presented in Section 3.2.

4.2.1. Single bubble yield dependence of liquid temperature

Numerical simulations of bubble oscillation and chemical reactions inside an isolated spherical air/water vapor bubble have been performed at various liquid temperatures (25–55 °C) when the ultrasonic frequency and acoustic intensity were maintained at 300 kHz and 2 W cm^{-2}. According to some experimental and theoretical data [49–52], the ambient radius (R_0) of a typical active bubble is strongly frequency dependent. The range of ambient bubble radius for a typical active bubble is rather narrow according to the experimental observations and it closes around a mean ambient radius [49,50]. The mean ambient bubble radius decreases considerably as ultrasonic frequency increases [49–52]. The ambient bubble radius (R_0) in the present numerical simulations has been assumed as the mean ambient bubble radius and the selected value was 5 μm at 300 kHz, according to some experimental and theoretical data results [50,52].

In Fig. 5(a)–(d), the calculated responses of the bubble characteristics to the fluctuation in the liquid pressure (for one acoustic period) have been shown for two different liquid temperatures (25 and 45 °C). The time axes in Fig. 5(a)–(d) are identical. The liquid pressure (Fig. 5(a)) applied on the bubble is the sum of the acoustic pressure and the static pressure. In Fig. 5(b), the evolution of bubble radius is shown. Starting from an ambient radius R_0, the bubble initially expands during the rarefaction part of the sound wave, reaching a maximum at the beginning of the compression phase, then quickly collapses during the compression part of ultrasound wave and expands again without any rebound. The bubble rebound depends on the experimental parameters, practically the frequency of ultrasound and the acoustic amplitude. At very high amplitude, such as that of our study, the bubble do not rebound but it enters directly in the successive rarefaction phase after each implosion. It can be seen from Fig. 5(b) that the bubble dynamic was slightly affected by the liquid temperature (the maximum radius and the bubble lifetime increased by only about 3% when the liquid temperature passes from 25 to 45 °C whereas, for the same conditions, the minimum bubble radius decreased by ~5%). In contrast, the intensity of the bubble implosion was strongly affected by the liquid temperature as can be seen in Fig. 5(c), which shows the velocity of the bubble wall as function of time during the whole lifetime of the bubble. The maximum velocity of the bubble wall decreased significantly, from 188 to 109 m s^{-1}, when the liquid temperature increased from 25 to 45 °C. This intense diminution in the speed of the bubble implosion affects considerably the maximum pressure and temperature attained in the bubble at the end of the bubble collapse. The maximum pressure in the bubble decreased from 1345 to 490 atm when the liquid temperature increased from 25 to 45 °C (Fig. 5(d)).

In Fig. 6(a)–(b), the calculated results of the bubble core temperature and the chemical reactions inside a bubble is shown as function of time at around the end of the bubble collapse, for the same condition as in Fig. 5. It is clearly seen that the maximum bubble temperature decreased from 4430 to 2715 K when the liquid temperature increased from 25 to 45 °C, respectively. This is due to the fact that as the liquid temperature increases the fraction of water vapor trapped in the bubble increases as a result of the rise of liquid vapor pressure with heating. This reduces γ of the mixture (γ_{H_2O} = 1.33 and γ_{air} = 1.4), which affects negatively the bubble core temperature (see Eq. (5)). The chemistry inside a bubble was also affected by the liquid temperature as a result of lowering bubble temperature. In fact, the number of the chemical reactions in the bubble decreased as the bubble temperature

Table 1
The important chemical reactions inside a collapsing air/water vapor bubble when the maximum bubble temperature is 4430 K, which is the maximum bubble temperature at 300 kHz when the bulk liquid temperature is 25 °C. This series of reactions are selected by analyzing the results of the chemical kinetics. M is the third body. Subscript "*f*" denotes the forward reaction and "*r*" denotes the reverse reaction. *A*, *b* and E_a are the Arrhenius parameters of the rate constant ($k = A\ b^n\ \exp(-E_a/RT)$ of each reaction. *A* is in ($cm^3\ mol^{-1}\ s^{-1}$) for two body reaction [($cm^6\ mol^{-2}\ s^{-1}$) for a three body reaction], and E_a is in (cal mol^{-1}).

No.	Chemical reaction	A_f	b_f	E_{af}	A_r	b_r	E_{ar}
1	$H_2O + M \leftrightarrow H^{\cdot} + {}^{\cdot}OH + M$	1.912×10^{23}	−1.83	1.185×10^5	2.2×10^{22}	−2.0	0.0
2	$O_2 + M \leftrightarrow O + O + M$	4.515×10^{17}	−0.64	1.189×10^5	6.165×10^{15}	−0.5	0.0
3	$H^{\cdot} + O_2 \leftrightarrow O + {}^{\cdot}OH$	1.915×10^{14}	0.0	1.644×10^4	5.481×10^{11}	0.39	-2.93×10^2
4	${}^{\cdot}OH + M \leftrightarrow O + H^{\cdot} + M$	9.88×10^{17}	−0.74	1.021×10^5	4.714×10^{18}	−1.0	0.0
5	$H^{\cdot} + O_2 + M \leftrightarrow HO_2^{\cdot} + M$	1.475×10^{12}	0.6	0.0	3.09×10^{12}	0.53	4.887×10^4
6	$O + H_2O \leftrightarrow {}^{\cdot}OH + {}^{\cdot}OH$	2.97×10^6	2.02	1.34×10^4	1.465×10^5	2.11	-2.904×10^3
7	$HO_2^{\cdot} + O \leftrightarrow {}^{\cdot}OH + O_2$	3.25×10^{13}	0.0	0.0	3.252×10^{12}	0.33	5.328×10^4
8	$HO_2^{\cdot} + H^{\cdot} \leftrightarrow {}^{\cdot}OH + {}^{\cdot}OH$	7.079×10^{13}	0.0	2.95×10^2	2.027×10^{10}	0.72	3.684×10^4
9	$O + H_2 \leftrightarrow H^{\cdot} + {}^{\cdot}OH$	3.82×10^{12}	0.0	7.948×10^3	2.667×10^4	2.65	4.88×10^3
10	$H^{\cdot} + H_2O \leftrightarrow {}^{\cdot}OH + H_2$	2.298×10^9	1.40	1.832×10^4	2.16×10^8	1.52	3.45×10^3
11	$H_2O + HO_2^{\cdot} \leftrightarrow H_2O_2 + {}^{\cdot}OH$	1.838×10^{10}	0.59	3.089×10^4	1.0×10^{12}	0.0	0.0
12	$HO_2^{\cdot} + {}^{\cdot}OH \leftrightarrow H_2O + O_2$	2.89×10^{13}	0.0	-4.97×10^2	5.861×10^{13}	0.24	6.908×10^4
13	$H_2 + HO_2^{\cdot} \leftrightarrow H_2O_2 + H^{\cdot}$	1.041×10^{11}	0.70	2.395×10^4	6.025×10^{13}	0.0	7.95×10^3
14	${}^{\cdot}OH + HO_2^{\cdot} \leftrightarrow H_2O_2 + O$	8.66×10^3	2.68	1.856×10^4	9.550×10^6	2.0	3.97×10^3
15	${}^{\cdot}OH + {}^{\cdot}OH + M \leftrightarrow H_2O_2 + M$	2.951×10^{14}	0.0	4.843×10^4	1.0×10^{14}	−0.37	0.0
16	$H_2O_2 + {}^{\cdot}OH \leftrightarrow H_2O + HO_2^{\cdot}$	1.0×10^{12}	0.0	0.0	1.838×10^{10}	0.59	3.089×10^4
17	$O_2 + O + M \leftrightarrow O_3 + M$	4.1×10^{12}	0.0	-2.114×10^3	2.48×10^{14}	0.0	2.286×10^4
18	$OH + O_2 \leftrightarrow O_3 + H$	4.4×10^7	1.44	7.72×10^4	2.3×10^{11}	0.75	0.0
19	$O + N_2 \leftrightarrow NO + N$	7.60×10^{13}	0.0	7.60×10^4	1.60×10^{13}	0.0	0.00
20	$NO + HO_2^{\cdot} \leftrightarrow OH + NO_2$	3.0×10^{12}	0.5	2.4×10^3	1.0×10^{11}	0.5	1.2×10^4
21	$NO_2 + M \leftrightarrow O + NO + M$	1.1×10^{16}	0.0	6.6×10^4	1.1×10^{15}	0.0	-1.88×10^3
22	$NO_2 + NO_2 \leftrightarrow NO + NO_3$	3.90×10^{11}	0.0	2.400×10^4	4.1×10^{14}	0.0	9.62×10^2
23	$NO_2 + O + M \leftrightarrow NO_3 + M$	1.1×10^{19}	0.0	0.0	2.5×10^9	0.0	0.0
24	$NO_3 + H \leftrightarrow OH + NO_2$	3.5×10^{14}	0.0	1.5×10^3	–	–	–
25	$N_2 + O + M \leftrightarrow N_2O + M$	1.40×10^{12}	0.0	2.08×10^4	5.0×10^{14}	0.0	5.8×10^4
26	$N_2 + O_2 \leftrightarrow N_2O + O$	6.3×10^{13}	0.0	1.104×10^5	1.0×10^{14}	0.0	2.82×10^4
27	$N_2O + H \leftrightarrow +N_2 + OH$	6.7×10^{13}	0.0	1.52×10^4	2.5×10^{12}	0.0	7.8×10^4
28	$OH + NO + M \leftrightarrow HNO_2 + M$	$8.\ 0 \times 10^{15}$	0.0	-1.0×10^3	5.10×10^{17}	−1.0	5.000×10^4
29	$HNO_2 + H \leftrightarrow H_2 + NO_2$	4.9×10^{11}	0.5	3.00×10^3	2.40×10^{13}	0.0	2.90×10^4
30	$H_2O + NO_2 \leftrightarrow OH + HNO_2$	8.40×10^{11}	0.0	4.227×10^4	1.5×10^{12}	0.0	5.60×10^1
31	$OH + NO_2 + M \leftrightarrow HNO_3 + M$	5.0×10^{17}	0.0	0.0	1.6×10^{15}	0.0	3.08×10^4
32	$O + HNO_2 \leftrightarrow HNO + O_2$	3.0×10^{12}	0.0	1.60×10^4	–	–	–
33	$HNO + M \leftrightarrow H + NO + M$	3.0×10^{16}	0.0	4.9×10^4	5.4×10^{15}	0.0	-3.0×10^2
34	$HNO + O \leftrightarrow OH + NO$	4.9×10^{11}	0.5	2.0×10^3	–	–	–
35	$HNO + H \leftrightarrow H_2 + NO$	4.8×10^{12}	0.0	0.0	1.4×10^{13}	0.0	5.526×10^4
36	$HNO + OH \leftrightarrow NO + H_2O$	6.3×10^{13}	0.0	0.0	2.40×10^6	0.0	5.0×10^3

Table 2
The important chemical reactions inside a collapsing air/water vapor bubble when the maximum bubble temperature is 2715 K, which is the maximum temperature of the bubble at 300 kHz when the bulk liquid temperature is 45 °C. This series of reactions are selected by analyzing the results of the chemical kinetics. M is the third body. Subscript "*f*" denotes the forward reaction and "*r*" denotes the reverse reaction. *A* is in ($cm^3\ mol^{-1}\ s^{-1}$) for two body reaction [($cm^6\ mol^{-2}\ s^{-1}$) for a three body reaction], and E_a is in (cal mol^{-1}).

No.	Chemical reaction	A_f	b_f	E_{af}	A_r	b_r	E_{ar}
1	$H_2O + M \leftrightarrow H^{\cdot} + {}^{\cdot}OH + M$	1.912×10^{23}	−1.83	1.185×10^5	2.2×10^{22}	−2.0	0.0
2	$H^{\cdot} + O_2 \leftrightarrow O + {}^{\cdot}OH$	1.915×10^{14}	0.0	1.644×10^4	5.481×10^{11}	0.39	-2.93×10^2
3	$H^{\cdot} + O_2 + M \leftrightarrow HO_2^{\cdot} + M$	1.475×10^{12}	0.6	0.0	3.09×10^{12}	0.53	4.887×10^4
4	$O + H_2O \leftrightarrow {}^{\cdot}OH + {}^{\cdot}OH$	2.97×10^6	2.02	1.34×10^4	1.465×10^5	2.11	-2.904×10^3
5	$HO_2^{\cdot} + {}^{\cdot}OH \leftrightarrow H_2O + O_2$	2.89×10^{13}	0.0	-4.97×10^2	5.861×10^{13}	0.24	6.908×10^4
6	$O + H_2 \leftrightarrow H^{\cdot} + {}^{\cdot}OH$	3.82×10^{12}	0.0	7.948×10^3	2.667×10^4	2.65	4.88×10^3
7	$H^{\cdot} + H_2O \leftrightarrow {}^{\cdot}OH + H_2$	2.298×10^9	1.40	1.832×10^4	2.16×10^8	1.52	3.45×10^3
8	$H_2O + HO_2^{\cdot} \leftrightarrow H_2O_2 + {}^{\cdot}OH$	1.838×10^{10}	0.59	3.089×10^4	1.0×10^{12}	0.0	0.0
9	$O_2 + O + M \leftrightarrow O_3 + M$	4.1×10^{12}	0.0	-2.114×10^3	2.48×10^{14}	0.0	2.286×10^4
10	$O + N_2 \leftrightarrow NO + N$	7.60×10^{13}	0.0	7.60×10^4	1.60×10^{13}	0.0	0.00
11	$N_2 + OH \leftrightarrow N_2O + H$	2.5×10^{12}	0.0	7.8×10^4	6.7×10^{13}	0.0	1.52×10^4
12	$NO + HO_2^{\cdot} \leftrightarrow OH + NO_2$	3.0×10^{12}	0.5	2.4×10^3	1.0×10^{11}	0.5	1.2×10^4
13	$NO_2 + M \leftrightarrow O + NO + M$	1.1×10^{16}	0.0	6.6×10^4	1.1×10^{15}	0.0	-1.88×10^3
14	$NO_2 + O + M \leftrightarrow NO_3 + M$	1.1×10^{19}	0.0	0.0	2.5×10^9	0.0	0.0
15	$NO_3 + H \leftrightarrow OH + NO_2$	3.5×10^{14}	0.0	1.5×10^3	–	–	–
16	$OH + NO + M \leftrightarrow HNO_2 + M$	8.0×10^{15}	0.0	-1.0×10^3	5.10×10^{17}	−1.0	$5.000 \times \times 10^4$
17	$H_2O + NO_2 \leftrightarrow OH + HNO_2$	8.40×10^{11}	0.0	4.227×10^4	1.5×10^{12}	0.0	5.60×10^1
18	$H_2O + NO_2 \leftrightarrow OH + HNO_2$	8.40×10^{11}	0.0	4.227×10^4	1.5×10^{12}	0.0	5.60×10^1
19	$OH + NO_2 + M \leftrightarrow HNO_3 + M$	5.0×10^{17}	0.0	0.0	1.6×10^{15}	0.0	3.08×10^4

decreased as can be seen in Tables 1 and 2 that summarized the important chemical reactions inside the bubble at two maximum bubble temperatures, 4430 and 2715 K, corresponding to, respectively, 25 and 45 °C of bulk liquid temperatures. The reaction schemes included in Tables 1 and 2 are refined from 73 possible reactions [42] according to the importance of each reaction toward the production/consumption of the main oxidizing species (·OH, O, $HO_2^{\cdot}$, H_2O_2 and O_3). The criterion of refining is that each

Table 3
Production rates of H_2O_2 in sonicated water as function of liquid temperature (conditions: volume: 300 mL, liquid temperature: 25–55 °C, frequency: 300 kHz, acoustic intensity: 2 W cm^{-2}).

Liquid temperature (°C)	25	35	45	55
H_2O_2 production rate (μM min^{-1})	2.50	3.25	3.65	4.00

reaction that contributes at less than 5% in the production or consumption of each oxidizing species is excluded. The most dominant products (detected at last at 10^{-17} mol) created in the bubble from the reactions of water vapor, O_2 and N_2 are (classified in descending order with respect to their maximum amount attained at the end of the bubble collapse): $H_2 > HNO_2 > {}^{\cdot}OH > O > NO > H^{\cdot} > HO_2^{\cdot} > HNO$ at 4430 K and ${}^{\cdot}OH > H_2 > O > H^{\cdot} > HO_2^{\cdot}$ at 2715 K. Thus, in all cases ·OH radical is the main radical oxidant detected in the bubble at appreciable amount. This highly reactive species has been specifically identified in sonicated aqueous solution via electron spin resonance [53]. Hence, the results of the numerical simulations may also be used to confirm that ·OH radical is the main species responsible for the sonochemical degradation of the three dyes (RhB, AO7 and MG).

In Fig. 7, the effect of liquid temperature in the range of 25–55 °C on the amount of ·OH radicals formed inside a collapsing single bubble and the number of active bubbles are shown for the same operational conditions as in Fig. 4. In this figure, the amount of ·OH radicals is defined by the maximum amount of ·OH radicals attained in the bubble at the end of the bubble collapse (see Fig. 6) as we assume that the bubble will fragments at this point (see Section 3.2). It was seen that the production of ·OH increases as the liquid bulk temperature increases from 25 to 35 °C and then decreases with further increase in the bulk liquid temperature. An interesting discussion about the existence of an optimum bulk liquid temperature for the production of ·OH inside a single bubble have been made elsewhere [54]. In short, the trend was resulted from the competition between two important parameters: the amount of water vapor trapped in the bubble at the collapse and the maximum bubble temperature achieved at the end of the bubble collapse. As the bulk liquid temperature increases, the liquid vapor pressure increases and consequently more water vapor is trapped in the bubble at the collapse (see Fig. 7 in Ref. [54]). This can promote the formation of free radicals coming from the dissociation of water vapor molecules. But increasing liquid temperature simultaneously involves less violent collapse (decreasing γ of the gas mixture) leading to lower internal bubble temperature at the end of the bubble collapse [54], which reduces the decomposition of molecules into free radicals. These two competing effects conduct to an optimum bulk liquid temperature for the production of ·OH as shown in Fig. 7.

From Fig. 7, it was also seen that an increase in bulk liquid temperature leads to a substantial increase in the number of active bubbles, which suggests that cavitation bubbles are more easily produced as the temperature is raised. This is in fact may be due to the decrease in cavitation threshold with the increase in liquid temperature as a result of the rise in vapor pressure or the decrease in either the surface tension or viscosity associated with heating of the liquid [55]. To the best of our knowledge, the effect of liquid temperature on the bubble number in acoustic cavitation field have been never investigated previously neither experimentally nor theoretically, but it is very accepted that the raise in the liquid temperature produces more cavitation bubbles [18,55].

In Fig. 8, the predicted overall production rate of ·OH radicals, which was obtained by multiplying the single bubble yield by the number of bubbles, is shown as function of bulk liquid temperature. The calculated overall production rate of ·OH radicals increased with increasing liquid temperature in the range 25–55 °C, showing a good agreement with the overall experimental trend observed in Fig. 4 concerning the degradation rate of RhB, AO7 and MG and Table 2 concerning the production rate of H_2O_2 with respect to the bulk liquid temperature. This indicates that of the two factors, the singe-bubble event and the number of active bubbles, the number of active bubbles must be the dominant factor that governs the effect of liquid temperature in the range 35–55 °C whereas both factors contributed to the enhancing effect of liquid temperature in the range 25–35 °C. As a consequence, the effect of liquid temperature on the sonochemical degradation in aqueous

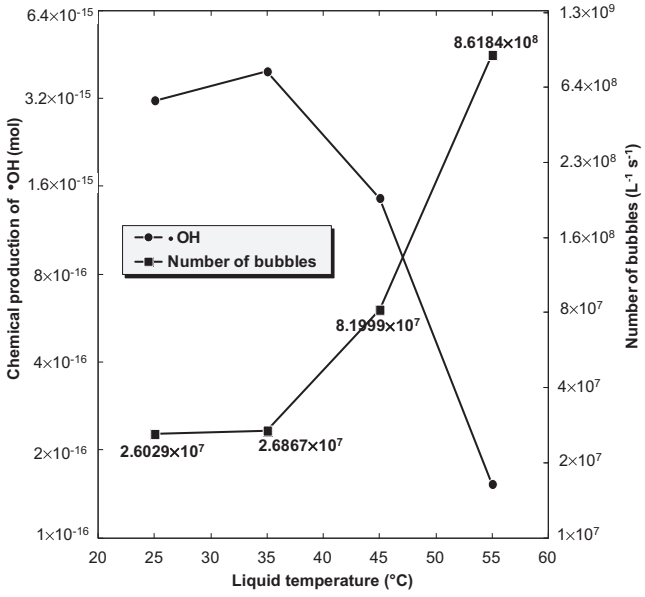

Fig. 7. The calculated chemical yield of ·OH for a single bubble and the number of active bubbles as function of liquid temperature (conditions: ambient bubble radius: 5 μm, driving frequency: 300 kHz, acoustic intensity: 2 W cm^{-2}, liquid temperature: 25–55 °C, static pressure: 1 atm). The vertical axes are in logarithmic scale.

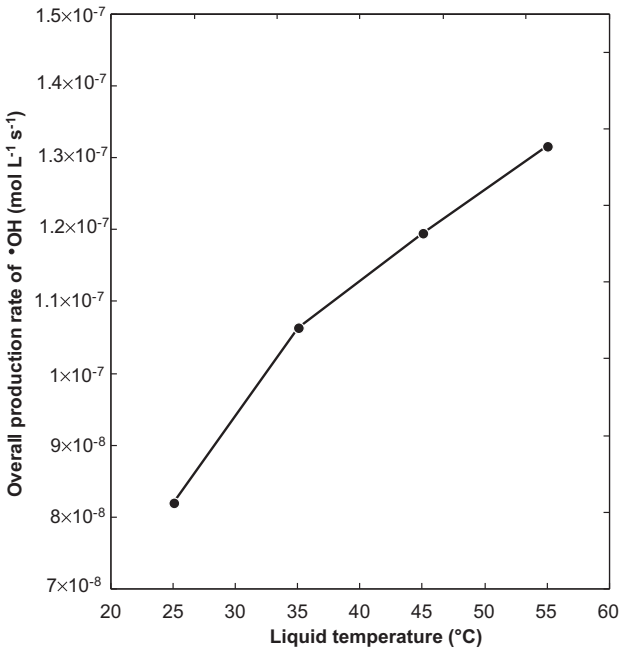

Fig. 8. The calculated overall production rate of ·OH radical as function of liquid temperature for the same conditions as in Fig. 7.

phase was controlled by the number of active bubbles in the range 35–55 °C and by the number of bubbles and the single bubble yield in the range 25–35 °C.

5. Conclusion

In this paper, the sonochemical degradation of three dyes: Rhodamine B (RhB), Acid orange 7 (AO7) and Malachite green (MG), frequently used in textile, was investigated at 300 kHz and for various liquid temperatures in the range 25–55 °C. The obtained results were discussed using a new comprehensive approach that combines the prediction of the single bubble yield and the number of active bubbles. The effects of bulk liquid temperature on the single bubble yield and the number of reacting bubbles have been evaluated for the same experimental conditions. The numerical simulation indicated that the production of ·OH radical from a single bubble presents an optimum at 35 °C of liquid temperature whereas the number of bubbles increases substantially with the increase in liquid temperature in the range 25–55 °C. As the degradation rate of dyes increased with the increase in liquid temperature in the range 25–55 °C, the following conclusions have been made:

- For the range 25–35 °C of liquid temperature, the sonolytic degradation rate of the dyes was controlled by both the singe-bubble event and the number of active bubbles,
- For the range 35–55 °C, the number of bubbles was the only factor that control the effect of liquid temperature on the sonochemical degradation rate of the dyes.

Finally, the present study provides a theoretical method that is easy to manipulate and that can give a prediction of single bubble yield and the number of bubbles for large interval of liquid temperatures, which allows a more realistic interpretations of the effects of this parameter on the sonochemical degradation of pollutants in aqueous liquids.

Acknowledgements

The financial support by the Ministry of Higher Education and Scientific Research of Algeria (project No. A16N01UN230120130010) is greatly acknowledged.

References

[1] T.J. Mason, C. Pétrier, Advanced oxidation processes for water and wastewater treatment, in: S. Parson (Ed.), Ultrasound Processes, IWA Publishing, London, 2004, pp. 185–208.
[2] M.R. Hoffmann, I. Hua, R. Höchemer, Application of ultrasonic irradiation for the degradation of chemical contaminants in water, Ultrason. Sonochem. 3 (1996) S163–S172.
[3] C. Pétrier, Y. Jiang, M.-F. Lamy, Ultrasound and environment: sonochemical destruction of chloroaromatic derivatives, Environ. Sci. Technol. 32 (1998) 1316–1318.
[4] M. Goel, H. Hongqiang, A.S. Mujumdar, M.B. Ray, Sonochemical decomposition of volatile and non–volatile organic compounds—a comparative study, Water Res. 38 (2004) 4247–4261.
[5] N.H. Ince, I. Gültekin, G. Tezcanli-Güyer, Sonochemical destruction of nonylphenol: effects of pH and hydroxyl radical scavengers, J. Hazard. Mater. 127 (2009) 739–743.
[6] T.G. Leighton, The Acoustic Bubble, Academic press, London, UK, 1994.
[7] K.S. Suslick, Y. Didenko, M.M. Fang, T. Hyeon, K.J. Kolbeck, W.B. McNamara, M. M. Mdleleni, M.M. Wong, Acoustic cavitation and its chemical consequences, Philos. Trans. R. Soc. A: Math. Phys. Eng. Sci. 357 (1999) 335–353.
[8] K.S. Suslick, D.A. Hammerton, R.E.J. Cline, Sonochemical hotspot, J. Am. Chem. Soc. 108 (1986) 5641–5642.
[9] K.S. Suslick, D.J. Flannigan, Inside a collapsing bubble: sonoluminescence and the conditions during cavitation, Annu. Rev. Phys. Chem. 59 (2008) 659–683.
[10] L.H. Thompson, L.K. Doraiswamy, Sonochemistry: science and engineering, Ind. Eng. Chem. Res. 38 (1999) 1215–1249.
[11] P. Riesz, D. Berdahl, C.L. Christman, Free radical generation by ultrasound in aqueous and nonaqueous solutions, Environ. Health Perspect. 64 (1985) 233–252.
[12] Y.G. Adewuyi, Sonochemistry: environmental science and engineering applications, Ind. Eng. Chem. Res. 40 (2001) 4681–4715.
[13] C. Pétrier, A. Francony, Ultrasonic wastewater treatment: incidence of ultrasonic frequency on the rate of phenol and carbon tetrachloride degradation, Ultrason. Sonochem. 4 (1997) 295–300.
[14] M.A. Beckett, I. Hua, Impact of ultrasonic frequency on aqueous sonoluminescence and sonochemistry, J. Phys. Chem. A 105 (2001) 3796–3802.
[15] F. Méndez-Arriaga, R.A. Torres, C. Pétrier, S. Esplugas, J. Gimenez, C. Pulgarin, Ultrasonic treatment of water contaminated with ibuprofen, Water Res. 42 (2008) 4243–4248.
[16] R.A. Torres, C. Pétrier, E. Combet, M. Carrier, C. Pulgarin, Ultrasonic cavitation applied to the treatment of bisphenol A. effect of sonochemical parameters and analysis of BPA by-products, Ultrason. Sonochem. 15 (2008) 605–611.
[17] M. Dukkanci, M. Vinatoru, T.J. Maison, Sonochemical treatment of orange II using ultrasound at range of frequencies and powers, J. Adv. Oxid. Technol. 15 (2012) 277–283.
[18] M.H. Entezari, P. Kruus, Effect of frequency on sonochemical reactions II: temperature and intensity effects, Ultrason. Sonochem. 3 (1996) 1924.
[19] Y. Jiang, C. Petrier, T.D. Waite, Sonolysis of 4-chlorophenol in aqueous solution: effects of substrate concentration, aqueous temperature and ultrasonic frequency, Ultrason. Sonochem. 13 (2006) 415–422.
[20] H. Ghodbane, O. Hamdaoui, Degradation of Acid Blue 25 in aqueous media using 1700 kHz ultrasonic irradiation: ultrasound/Fe(II) and ultrasound/H_2O_2 combinations, Ultrason. Sonochem. 16 (2009) 593–598.
[21] S. Merouani, O. Hamdaoui, F. Saoudi, M. Chiha, Sonochemical degradation of Rhodamine B in aqueous phase: effects of additives, Chem. Eng. J. 158 (2010) 550–557.
[22] R. Jain, M. Mathur, S. Sikarwar, A. Mittal, Removal of the hazardous dye rhodamine B through photocatalytic and adsorption treatments, J. Environ. Manage. 85 (2007) 956–964.
[23] H.F. Mark, O.F. Othmer, C.G. Overbrger, G.T. Seaborg, Encyclopedia of Chemical Technology, vol. 3, John Wiley and Sons, USA, 1978. pp. 387–406.
[24] G. Crini, H.N. Peindy, F. Gimbert, C. Robert, Removal of C.I. Basic Green 4 (Malachite Green) from aqueous solutions by adsorption using cyclodextrin based adsorbent: kinetic and equilibrium studies, Sep. Purif. Technol. 53 (2007) 97–110.
[25] O. Moumeni, O. Hamdaoui, Intensification of sonochemical degradation of malachite green by bromide ions, Ultrason. Sonochem. 19 (2012) 404–409.
[26] C. Berberidou, I. Poulios, N.P. Xekoukoulotakis, D. Mantzavinos, Sonolytic, photocatalytic and sonophotocatalytic degradation of malachite green in aqueous solutions, Appl. Catal. B 74 (2007) 63–72.
[27] S. Merouani, O. Hamdaoui, Y. Rezgui, M. Guemini, A method for predicting the number of active bubbles in sonochemical reactors, Ultrason. Sonochem. 22 (2015) 51–58.
[28] T.J. Mason, J.P. Lorimer, D.M. Bates, Quantifying sonochemistry: casting some light on a 'black art', Ultrasonics 30 (1992) 40–42.
[29] S. Koda, T. Kimura, T. Kondo, H. Mitome, A standard method to calibrate sonochemical efficiency of an individual reaction system, Ultrason. Sonochem. 10 (2003) 149–156.
[30] C. Kormann, D.W. Bahnemann, M.R. Hoffmann, Photocatalytic production of H_2O_2 and organic peroxides in aqueous suspensions of TiO_2, ZnO, and desert sand, Environ. Sci. Technol. 22 (1988) 798–806.
[31] S. Merouani, O. Hamdaoui, Y. Rezgui, M. Guemini, Theoretical estimation of the temperature and pressure within collapsing acoustical bubbles, Ultrason. Sonochem. 21 (2014) 53–59.
[32] S. Merouani, O. Hamdaoui, Y. Rezgui, M. Guemini, Modeling of acoustic cavitation as an advanced technique for water treatment, Desalin. Water Treat. (2014), http://dx.doi.org/10.1080/19443994.2014.950994. in press.
[33] L.A. Crum, The polytrophic exponent of gas contained within air bubbles pulsating in a liquid, J. Acoust. Soc. Am. 73 (1983) 116–120.
[34] J.B. Keller, I.I. Kolodner, Damping of underwater explosion bubble oscillations, J. Appl. Phys. 27 (1956) 1152–1161.
[35] J.B. Keller, M.J. Miksis, Bubble oscillations of large amplitude, J. Acoust. Soc. Am. 68 (1980) 628–633.
[36] A.J. Colussi, L.K. Weavers, M.R. Hoffmann, Chemical bubble dynamics and quantitative sonochemistry, J. Phys. Chem. A 102 (1998) 6927–6934.
[37] N.P. Vichare, P. Senthilkumar, V.S. Moholkar, P.R. Gogate, A.B. Pandit, Energy analysis in acoustic cavitation, Ind. Eng. Chem. Res. 39 (2000) 1480–1486.
[38] K. Yasui, Effect of non-equilibrium evaporation and condensation on bubble dynamics near the sonoluminescence threshold, Ultrasonics 36 (1998) 575–580.
[39] B.D. Storey, A.J. Szeri, Water vapor, sonoluminescence and sonochemistry, Proc. R. Soc. Lond. A 456 (2000) 1685–1709.
[40] V. Kamath, A. Prosperetti, F.N. Egolfopoulos, A theoretical study of sonoluminescence, J. Acoust. Soc. Am. 94 (1993) 248–260.
[41] S. Fujikawa, T. Akamatsu, Effects of the non-equilibrium condensation of vapour on the pressure wave produced by the collapse of a bubble in a liquid, J. Fluid Mech. 97 (1980) 481–512.
[42] S. Merouani, O. Hamdaoui, Y. Rezgui, M. Guemini, Sensitivity of free radicals production in acoustically driven bubble to the ultrasonic frequency and nature of dissolved gases, Ultrason. Sonochem. 22 (2015) 41–50.

[43] M. Chiha, S. Merouani, O. Hamdaoui, S. Baup, N. Gondrexon, C. Pétrier, Modeling of ultrasonic degradation of non-volatile organic compounds by Langmuir-type, Ultrason. Sonochem. 17 (2010) 773–782.
[44] Datasheet of Acid orange 7 in Chemicalland21, http://www.chemicalland21.com/specialtychem/finechem/ORANGE%20II.htm.
[45] Datasheet of Malachite green in PubChem open chemistry database, https://pubchem.ncbi.nlm.nih.gov/compound/Malachite_Green_Oxalate#section=Top.
[46] The Good Scents Company Information System, http://www.thegoodscentscompany.com/episys/ep1270901.html.
[47] Datasheet of Malachite green in GuidChem database, http://www.guidechem.com/reference/dic-609234.html.
[48] A. Mehrdad, R. Hashemzadeh, Ultrasonic degradation of Rhodamine B in the presence of hydrogen peroxide and some metal oxide, Ultrason. Sonochem. 17 (2010) 168–172.
[49] A. Brotchie, F. Grieser, M. Ashokkumar, Effect of power and frequency on bubble-size distributions in acoustic cavitation, Phys. Rev. Lett. 102 (2009) 084302-1–084302-4.
[50] S. Labouret, J. Frohly, Distribution en tailles des bulles d'un champ de cavitation ultrasonore, 10ème Congrès Français d'Acoustique, Lyon, 2010, http://hal.archives-ouvertes.fr/docs/00/55/11/51/PDF/000441.pdf.
[51] K. Yasui, Influence of ultrasonic frequency on multibubble sonoluminescence, J. Am. Chem. Soc. 112 (2002) 1405–1413.
[52] S. Merouani, O. Hamdaoui, Y. Rezgui, M. Guemini, Effects of ultrasound frequency and acoustic amplitude on the size of sonochemically active bubbles – theoretical study, Ultrason. Sonochem. 20 (2013) 815–819.
[53] K. Makino, M.M. Mossoba, P. Riesz, Chemical effects of ultrasound on aqueous solutions. Formation of hydroxyl radicals and hydrogen atoms, J. Phys. Chem. 87 (1983) 1369–1377.
[54] S. Merouani, O. Hamdaoui, Y. Rezgui, M. Guemini, Computer simulation of chemical reactions occurring in collapsing acoustical bubble: dependence of free radicals production on operational conditions, Res. Chem. Intermed. (2013), http://dx.doi.org/10.1007/s11164-013-1240-y.
[55] T.J. Mason, J.P. Lorimer, Applied Sonochemistry: The Use of Power Ultrasound in Chemistry and Processing, Wiley-VCH Verlag GmbH, Weinheim, 2002. pp. 198–214.